Coherent Plasmon and Phonon-Plasmon Resonances in Carbon Nanotubes

Abram L. Falk,[1,*] Kuan-Chang Chiu,[1,2] Damon B. Farmer,[1] Qing Cao,[1] Jerry Tersoff,[1] Yi-Hsien Lee,[2] Phaedon Avouris,[1] and Shu-Jen Han[1]

[1]IBM T. J. Watson Research Center, Yorktown Heights, New York 10598, USA

[2]Department of Materials Science and Engineering, National Tsing-H 13

(Received 3 December 2016; published 22 June 2017)

Carbon nanotubes provide a rare access point into the plasmon physics of one-dimensional electronic systems. By assembling purified nanotubes into uniformly sized arrays, we show that they support coherent plasmon resonances, that these plasmons couple to nanotube and substrate phonons, and that the resulting phonon-plasmon resonances have quality factors as high as 10. Because nanotube plasmons intensely strengthen electromagnetic fields and light-matter interactions, they provide a compelling platform for surface-enhanced spectroscopy and tunable optical devices at deep-subwavelength scales.

DOI: 10.1103/PhysRevLett.118.257401

Plasmons in carbon nanotubes [1–5] comprise longitudinal-charge oscillations coupled to infrared or terahertz optical fields. They can either propagate [3–5] or be confined to Fabry–Pérot resonators by reflections at the nanotube ends [6–10] [F . 1(a)]. Propagation losses are low [3], and the resonant frequencies and absorption coefficients can be controlled via the length [8,10] a l [7,9] of the nanotubes. The strong confinement of electromagnetic fields deriving from the nanotubes' one dimensionality could allow light to be guided at the nanometer scale and light-matter interactions to be enhanced by Purcell factors predicted to be as high as 10^6 [5].

At infrared frequencies, nanotube plasmonics could lead to highly sensitive absorption spectroscopy through surface-enhanced infrared absorption (SEIRA) [11–13]. At terahertz frequencies, it could enable tunable lasers and receivers for use in terabit-per-second wireless communications [14–16]. Ult lasmonic circuitry could be naturally integrated with high-performance nanotube transistors.

However, nanotube plasmonics has been frustrated by the material quality of nanotube films. In inhomogeneous nanotube films, with a broad distribution of lengths, diameters, and/or doping levels, plasmons resonating at different frequencies quickly lose phase coherence with each other, leading to fast dissipation. The quality (Q) factor, which is the quotient of the resonant angula limited observations of nanot lasmon resonators to the incoherent $Q \ll 1$ regime [6–10]. Because dissipation constrains nearly all applications of plasmonics, the demonstration of high-Q resonators would provide crucial evidence that nanotubes are a technologically viable plasmonic material.

In this Letter, we show that coherent nanotube plasmon and phonon-plasmon resonances can have ensemble Q factors as high as 3 and 10, respectively. The key to our demonstration is our exceptionally uniform nanotube films, which we develop using a Langmuir-Schaeffer technique [17]. We conservatively estimate that our nanotube resonators confine an electromagnetic field whose free-space wavelength (λ_0) is 8 μm to a mode volume (V) of 0.002 μm^3. With this combination of Q and optical concentration ($\lambda_0^3/V = 300\,000$), the Purcell factor by which these plasmonic resonators could enhance light-matter interactions [18], $P = (3Q/4\pi^2)(\lambda_0^3/V)$, exceeds 100 000. As an illustration of a technology arising from this extraordinary enhancement, we demonstrate nanotube-based SEIRA spectroscopy. All of the assembly and fabrication processes developed in this Letter can be readily extended to the wafer scale.

The supporting substrates for our carbon nanotube films are Si with 10 nm of SiO_2 and 0, 10, or 40 nm of diamondlike carbon (DLC) on top of the SiO_2. The DLC is a nonpolar spacer that controls the coupling between plasmons in the nanotubes and polar phonons in the SiO_2. To assemble the nanotube films, we added 99.9% semiconducting

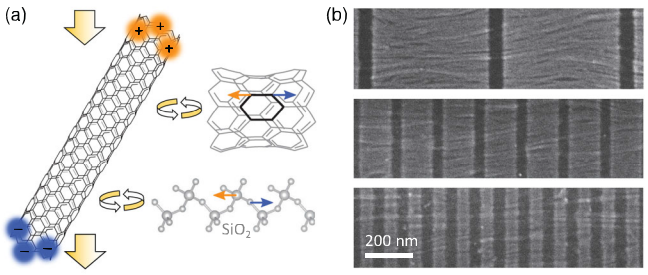

FIG. 1. (a) Finite-length nanotubes act as plasmonic Fabry-Pérot resonators. The plasmon resonances are excited with broad-spectrum infrared light in a micro Fourier-t (μ-FTIR) spectrometer. Before decaying, t

(b) Scanning electron micrographs of cut and aligned nanotube segments. The nanotube film thickness is 6 nm.

nanotubes in 1,2-dichloroethane to the wafer surface of a Langmuir trough. Mechanical moving bars compressed the suspension to a target pressure of 30 mN m^{-1} with a bar-moving rate of 20 cm^2 min^{-1} under multiple (~10) isothermal cycles. We transferred the 6-nm-thick nanotube arrays onto the various target substrates and used oxygen-based reactive-ion etching to cut the nanotubes into short segments, whose length (L) ranged from 30 to 500 nm [F (b)]. We then exposed them to NO_2 gas, a strong oxidizer that induces positive free charge carriers in the nanotubes [19], and studied the plasmon resonances with μ-FTIR at room temperature. Each measurement spatially averages 1-10 $\times$ 10^6 nanotubes in a ~(25 μm)^2 area.

We observe three prominent resonances from the nanot [Fig. 2(a)]. The frequency of the highest-frequency resonance (ν_1) conspicuously increases as the segment length (L) decreases, a behavior that identifies ν_1 as the Fabry-Pérot resonance of the nanotube plasmon. At $L = 30$ nm, ν_1 reaches 3000 cm^{-1}, corresponding to a free space wavelength of $\lambda_0 = 3$ μm. This result shows that nanotube plasmon resonances, previously observed at THz through far-infrared frequencies [6–10], can also span the midinfrared frequency range.

When we lithographically cut the nanotube films parallel to the nanotube alignment direction, not perpendicula [Fig. 2(b)]. This measurement confirms that uniform segmentation (i.e., length control) of the nanotubes is important to the coherence of their ensemble plasmon resonance. Moreover, the attenuation of light pola llel to the nanotube alignment direction ($A_\parallel$) is much stronger than that of perpendicularly polarized light ($A_\perp$), with $A_\parallel/A_\perp = 6 \pm 1$ [Fig. 2(b), inset]. The observed ratio indicates good, though imperfect, nanotube alignment.

A distinctive feature of nanotube plasmonic resonators is that their doping le l can dynamically control t litudes. Figures 2(c) and S3 [20] show that the doping level strongly affects the plasmon resonances, with a highly p-type doped film exhibiting a 6-times-stronger ν_1 attenuation peak than same film when undoped. Doping also causes ν_1 to blueshift from 1370 to 1920 cm^{-1}, a 40% change in frequency. In t lectrically gated nanot lasmons could lead to modula -frequency communications and tunable SEIRA spectrometers.

The frequency of the lower energy resonances (ν_2 and ν_3) evolve much more weakly with L than ν_1 does. However, their intensities and shapes are strong functions of L and, in particular, are strongly enhanced as the frequency of ν_1 approaches their frequencies. These behaviors indicate that they derive from plasmon-coupled phonons. By comparing the nanotubes' spectra to spectra of graphene nanoribbons on SiO_2, we identify ν_3 with the 1168-cm^{-1} longitudinal optical (LO) phonon in the SiO_2 substrate [16,22]. The ν_2 resonance at 1590 cm^{-1} corresponds to the infrared-a .

These phonon modes, though closely rela - band Raman modes of nanotubes [25], are ordinarily very weak spectroscopic features in an absorption measurement.

However, plasmon coupling significantly strengthens these phonon modes and modifies their shape (Fig. 3). For $L < 60$ nm, when ν_1 is significantly greater than 1590 cm^{-1}, ν_2 is absent. As L increases, the ν_2 feature appears as an attenuation peak. As L continues to increase, its line shape becomes asymmetric and then evolves into a

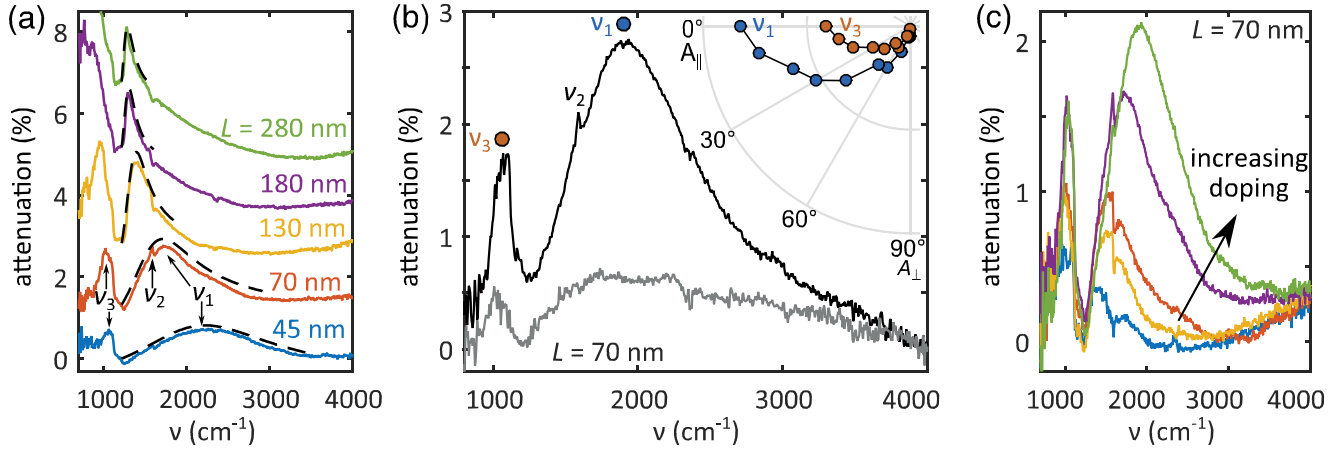

FIG. 2. (a) The attenuation spectra of nanotube resonators when directly resting on the SiO_2 substrate, showing both plasmon (ν_1) and plasmon-coupled phonon (ν_2 and ν_3) resonances. The spectra are sequentially vertically offset, for clarity, and the black dashed lines are fits to Fano functions. (b) Cut-direction dependence of the plasmonic absorption. The black (gray) curve is the attenuation spectrum of nanotubes cut perpendicula llel) to their alignment direction. Inset: polarization dependence of the intensity of peaks ν_1 and ν_3, with the cut direction fixed to be the perpendicular direction [as shown in Fig. 1(b)]. The intensities of peaks ν_1 and ν_3 are each 6 $\pm$ 1 times greater when the polarizer is oriented along the nanotube length rather than perpendicular to it. (c) Doping dependence of the nanotube segments. The green curve is measured immediately after NO_2 exposure. For each curve below it, the samples have rested in atmospheric conditions for one extra day, whereby the doping level decreases. The sheet charge densities range from approximately 10^{-8} C cm^{-2} to 10^{-6} C cm^{-2} [20].

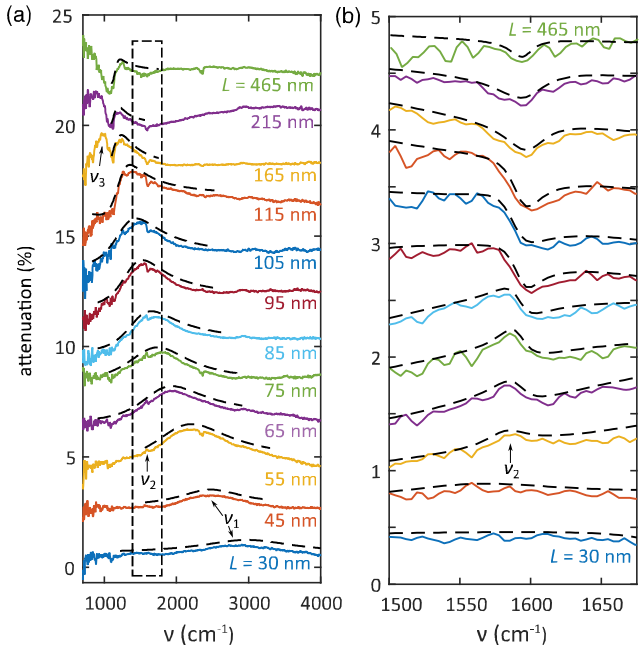

FIG. 3. (a) The attenuation spectra of nanotube segments on the 40-nm DLC substrate, showing ν_1 decreasing with increasing L and passing through the 1590-cm^{-1} nanotube phonon resonance. The spectra are sequentially vertically offset, for cla lack dashed lines are fits to Fano functions, which are also offset from the data. (b) A magnification of the dashed rectangle from Fig. 3(a), along with fits to Fano functions (black dashed lines), showing the 1590-cm^{-1} E_{1u} nanotube phonons when ν_1 is on or nearly on resonance. As L increases and ν_1 moves through the 1590-cm^{-1} resonance, t -cm^{-1} phonon resonance changes from being absent, to being an absorbing feature (due to constructive interference), to being a partially transparent feature (due to destructive interference). The fitted resonance width (γ_2) ranges from 20 to 30 cm^{-1}.

window of phonon-induced transparency. The intensity of ν_2 also evolves with the nanotube-doping level and is much stronger when ν_1 is on resonance [Fig. 2(c)]. This resonant enhancement demonstrates the principle of SEIRA spec- t ld be used to sensitively detect and probe nearby chemicals, including biomolecules.

The intensity of ν_3, the SiO_2 phonon resonance, also strongly increases as L increases and ν_1 approaches ν_3. Moreover, as can be seen in Fig. 2(a), while the line shape of ν_1 is symmetrical for the shortest nanotubes, it evolves into an increasingly asymmetrical line shape as ν_1 approaches ν_3. Understanding the line shapes to result from Breit-Wigner-Fano interference [26,27] between plasmon and phonon resonances, we fit all of the ν_1 and ν_2 line shapes to

$$A(\nu) \propto \frac{(F_j\gamma_j + \nu - \nu\ )^2}{(\nu-\nu_j)^2+\gamma_j^2} + b_j \qquad (1)$$

with A the attenuation, γ_j the linewidth, which is the damping rate divided by 2π, F_j the Fano parameter, which characterizes the resonance's degree of asymmetry, b_j an offset parameter that represents screening of the resonance by intrinsic losses [28], and $j = 1$ or 2. These fits exhibit excellent agreement with the measured spectra [Figs. 2(a), 3(a), and 3(b)]. We do not fit ν_3 line shapes in this Letter, because this peak, though primarily deriving from the 1168-cm^{-1} phonon in SiO_2, also shows interference from the 806-cm^{-1} longitudinal optical phonon in SiO_2. We cannot derive all of the rates describing the coupled phonon-plasmon coupling from our measured spectra alone, and the crossover from induced transparency to the strong-coupling or vacuum-Rabi-splitting regime is complex [29,30]. Nevertheless, because ν_2 is a much sharper feature than ν_1, we interpret it as phonon-induced transparency. The coupling between ν_1 and ν_3 is significantly stronger and, as we will show below, at the threshold of the strong-coupling regime.

When plotting ν_1 and ν_3 vs wave vector (q), where $q = \pi/L$, we observe a clear anticrossing [Fig. 4(a)]. In t -L (high-q) limit, ν_1 is asymptotically linear with q, consistent with the theory of plasmon resonances of one-dimensional electronic systems [1–3,31,32]. The slope of this linear asymptote in Fig. 4(a) (0.0032) implies an asymptotic effective index of refraction of $1/(2\pi \times 0.0032) = 50$ and a plasmon velocity (V_p) of $c/50$. In terms of the Fermi velocity ($V_F = c/300$), $V_p = 6V_F$.

The γ_1 linewidths and corresponding Q factors [Figs. 4(b)–(c)] a $\gamma_1^{-1} = \sim$200 fs. As L decreases, γ_1^{-1} decreases, reaching 50 fs for $L = 100$ nm and 20 fs for $L = 40$ nm. Calculating Q as ν_1/γ_1, we find that Q has a maximum of 10 and also decreases with decreasing L until $L < 100$ nm, at which point it remains an approximately constant $Q = 2$. Among plasmon resonances with minimal coupling to SiO_2 phonons, $Q = 3$ was the highest quality factor that we observed. The Q vs L trend derives from mult luding lithographic effects, nanotube alignment effects, an increased number of phonon decay pathways for higher-energy plasmons [16], and phonon-plasmon hybridization near ν_3. Coupled antenna theory also indicates that mutual coupling in dense nanotube arrays blueshifts and broadens ensemble plasmon resonances [33].

The frequency of the ν_1-ν_3 splitting at the 1168-cm^{-1} anticrossing corresponds to twice the plasmon-phonon coupling strength [g_{13}, see Fig. 4(d)]. As expected, g_{13} is highest (6.5 THz) when the nanotubes rest directly on the SiO_2. This coupling strength is comparable to the ~5-THz linewidth of ν_1 and ν_3 near their anticrossing, indicating that the ν_1-ν_3 interaction is at the threshold of the strong-coupling regime. Fitting g_{13} as a function of the DLC-spacer thickness (x) to $e^{-x/\delta}$ provides an estimate of the transverse decay length of the plasmon mode [Fig. 4(e)]. This length, $\delta = 55$ nm, is 150 times smaller than $\lambda_0 = 8.3\,\mu$m (1200 cm^{-1}) at $L = 180$ nm. We estimate the maximum Purcell factor at the mode center to be $P = 180\,000$ [20].

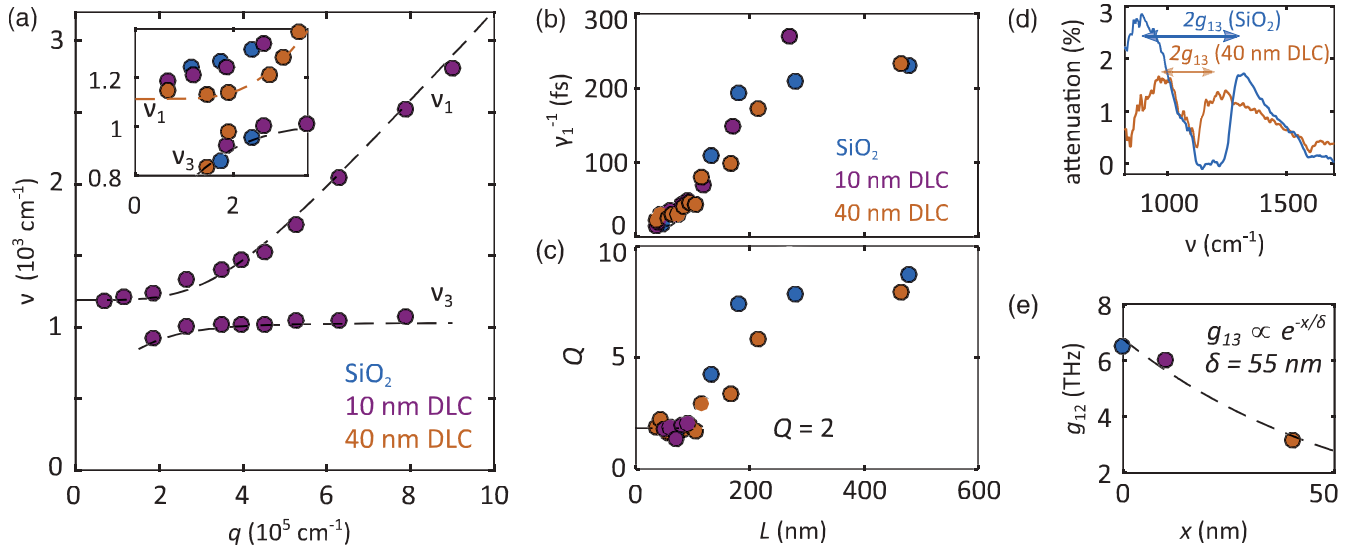

FIG. 4. (a) The resonant frequencies, ν_1 and ν_3, as a function of the wave vector ($q = \pi/L$). The dashed black lines are guides to the eye. The ν_1 frequencies derive from fits, and the ν_3 frequencies derive from selecting the frequency corresponding to the local maximum of the attenuation spectra. Inset: ν_1 and ν_3 vs q near the anticrossing at 1168 cm^{-1}. The splitting between ν_1 and ν_3 is smaller when the DLC spacer is larger. (b) γ_1^{-1}, derived from fits to Eq. (1) as a function of L. (c) Q, computed as ν_1/γ_1, as a function of L. (d) The attenuation spectrum at the anticrossing ($L = 180$ nm, $q = 1.8 \times 10^5$ cm^{-1}), showing a higher g_{13} splitting for the nanotubes resting on SiO_2 compared to those resting on the 40-nm DLC substrate. (e) g_{13} as a function of the DLC thickness (x).

Isola

ly high value [5,34].

The plasmon resonances of graphene nanoribbons [16,35–38] share several features with those that we observe in nanotubes, including plasmon-phonon hybridization [16] and phonon-induced transparency [36]. However, nanotube plasmonics has several unique advantages. The one dimensionality of nanotubes allows them to confine light to smaller volumes and to suffer from less scattering at edges [4,5]. Their linear dispersion relationship, compared to the square-root relationship for graphene [16,35], makes their resonances more broadly tunable. Highly absorptive thick films of nanotubes would have no clearly manufacturable analogue in graphene. Finally, compared to those of metallic graphene, the plasmon resonances of semiconducting nanotubes have both stronger doping effects and a potential to form more efficient photothermoelectric detectors [39].

In conclusion, we showed that carbon nanotubes can be a high-quality plasmonic nanomaterial that significantly strengthens light-matter interactions. As demonstrated by the resonant enhancement of phonons that we observe, nanotube plasmonics should be an ideal tool for sensitive SEIRA spectroscopy. In this application, nanotubes could play a dual role as plasmonic resonators and infrared receivers, and functionalization could enhance their interaction with specific analytes. Their nonlinearity and aniso- t l properties make them promising building blocks for metamaterials [40], and they could play a role in quantum optics by enhancing and tuning single-photon sources [41]. In the long run, because nanotubes can function both as electrical t

lators, they could be a foundation for integrating electrical and optical logic at the nanometer scale.

The authors thank Javier García de Abajo, Hendrik Hamann, Easwar Magesan, David Toyli, Joel Chudow, James Hannon, and Jianshi Tang for discussions, George Tulevski for performing the Raman and ultraviolet-visible spectroscopic characterization of the nanotubes, and Jim Bucchignano for performing the electron-beam lithography. This work was funded by IBM.

*alfalk@us.ibm.com

[1] G. Y. Slepyan, S. A. Maksimenko, A. Lakhtakia, O. Yevtushenko, and A. V. Gusakov, Electrodynamics of carbon nanotubes: Dynamic conductivity, impedance boundary conditions, and surface wave propagation, Phys. Rev. B **60**, 17136 (1999).

[2] T. Nakanishi and T. Ando, Optical response of finite-length carbon nanotubes, J. Phys. Soc. Jpn. **78**, 114708 (2009).

[3] Z. Shi, X. Hong, H. A. Bechtel, B. Zeng, M. C. Martin, K. Watanabe, T. Taniguchi, Y.-R. Shen, and F. Wang, Observation of a Luttinger-liquid plasmon in metallic single-walled carbon nanotubes, Nat. Photonics **9**, 515 (2015).

[4] I. S. Lamata, P. Alonso-Gonzalez, R. Hillenbrand, and A. Y. Nikitin, Plasmons in cylindrical 2D materials as a platform for nanophotonic circuits, ACS Photonics **2**, 280 (2015).

[5] L. Martin-Moreno, F. J. G. De Abajo, and F. J. Garcia-Vidal, Ultraefficient Coupling of a Quantum Emitter to the Tunable Guided Plasmons of a Carbon Nanotube, Phys. Rev. Lett. **115**, 173601 (2015).

[6] F li, L. Degiorgi, P. Wachter, W. S. Bacsa, W. A. De Heer, and L. Forro, Evidence of anisotropic metallic behaviour in the optical properties of carbon nanotubes, Solid State Commun. **99**, 513 (1996).

[7] N. Akima, Y. Iwasa, S. Brown, A. M. Barbour, J. Cao, J. L. Musfeldt, H. Matsui, N. Toyota, M. Shiraishi, H. Shimoda, and O. Zhou, Strong anisotropy in the far-infrared absorp- t -aligned single-walled carbon nano- t

[8] M. V. Shuba, A. G. Paddubskaya, A. O. Plyushch, P. P. Kuzhir, G. Y. Slepyan, S. A. Maksimenko, V. K. Ksenevich, P. Buka, D. Seliuta, I. Kasalynas, J. Macutkevic, G. Valusis, C. Thomsen, and A. Lakhtakia, Experimental evidence of localized plasmon resonance in composite materials containing single-wall ca (2012).

[9] Q. Zhang, E. H. Haroz, Z. Jin, L. Ren, X. Wang, R. S. Arvidson, A. Luttge, and J. Kono, Plasmonic nature of the terahertz conductivity peak in single-wall ca , Nano Lett. **13**, 5991 (2013).

[10] T -K. Joung, T. Saito, D. N. Futaba, K. Hata, and T. Okazaki, Length-dependent plasmon resonance in single-walled carbon nanotubes, ACS Nano **8**, 9897 (2014).

[11] A. Hartstein, J. R. Kirtley, and J. C. Tsang, Enhancement of the Infrared Absorption from Molecula layers with Thin Metal Overlayers, Phys. Rev. Lett. **45**, 201 (1980).

[12] D. B. Farmer, P. Avouris, Y. Li, T. F. Heinz, and S. Han, Ult lasmonic detection of molecules with graphene, ACS Photonics **3**, 553 (2016).

[13] F l, Y. A. Urzhumov, H. Wang, J. Kundu, N. J. Halas, J. Aizpurua, and P. Nordlander, Metallic nanoparticle arrays: A common substrate for both surface-enhanced Raman scattering and surface-enhanced infrared absorption, ACS Nano **2**, 707 (2008).

[14] X. He, W , Q. Zhang, L. Ren, and J. Kono, Carbon-based terahertz devices, Proc. SPIE Int. Soc. Opt. Eng. **9476**, 947612 (2015).

[15] X. He, N. Fujimura, J. M. Lloyd, K. J. Erickson, A. A. Talin, Q. Zhang, W. Gao, Q. Jiang, Y. Kawano, R. H. Hauge, F. Léonard, and J. Kono, Carbon nanotube terahertz detector, Nano Lett. **14**, 3953 (2014).

[16] H. Yan, T. Low, W. Zhu, Y. Wu, M. Freitag, X. Li, F. Guinea, P. Avouris, and F. Xia, Damping pathways of mid-infrared plasmons in graphene nanostructures, Nat. Photonics **7**, 394 (2013).

[17] Q. Cao, S. Han, G. S. Tulevski, Y. Zhu, D. D. Lu, and W. Haensch, Arrays of single-walled carbon nanotubes with full surface coverage for high-performance electronics, Nat. Nanotechnol. **8**, 180 (2013).

[18] R. F. Oulton, G. Bartal, D. F. P. Pile, and X. Zhang, Confinement and propagation characteristics of subwavelength plasmonic modes, New J. Phys. **10**, 105018 (2008).

[19] J. Kong, N. R. Franklin, C. Zhou, M. G. Chapline, S. Peng, K. Cho, and H. Dai, Nanotube molecula (2000).

[20] See Supplemental Material at http://link.aps.org/supplemental/10.1103/PhysRevLett.118.257401, which includes Ref. [21], for a more detailed discussion of experimental methods, fitting methods, and the effect of charge-transfer doping.

[21] R. B. Weisman and S. M. Bachilo, Dependence of optical t -walled carbon nanotubes in aqueous suspension: An empirical Kataura plot, Nano Lett. **3**, 1235 (2003).

[22] A. Kučírková and K. Navrátil, Interpretation of infrared transmittance spectra of SiO2 thin films, Appl. Spectrosc. **48**, 113 (1994).

[23] U. Kuhlmann, H. Jantoljak, N. Pfänder, P. Bernier, C. Journet, and C. Thomsen, Infrared active phonons in single-walled carbon nanotubes, Chem. Phys. Lett. **294**, 237 (1998).

[24] F I. Trembla . Tang, R. Martel, and P. Desjardins, Fano Resonances in the Mid-infrared Spectra of Single-Walled Carbon Nanotubes, Phys. Rev. Lett. **109**, 097402 (2012).

[25] M. S. Dresselhaus, G. Dresselhaus, R. Saito, and A. Jorio, Raman spectroscopy of carbon nanotubes, Phys. Rep. **409**, 47 (2005).

[26] U. Fano, Effects of configuration interaction on intensities and phase shifts, Phys. Rev. **124**, 1866 (1961).

[27] B. Luk'yanchuk, N. I. Zheludev, S. A. Maier, N. J. Halas, P. Nordlander, H. Giessen, and C. T. Chong, The Fano resonance in plasmonic nanostructures and metamaterials, Nat. Mater. **9**, 707 (2010).

[28] B. Gallinet and O. J. F. Martin, *Ab initio* theory of Fano resonances in plasmonic nanostructures and metamaterials, Phys. Rev. B **83**, 235427 (2011).

[29] P. M. Anisimov, J. P. Dowling, and B. C. Sanders, Objectively Discerning Autler-Townes Splitting from Electromagnetically Induced Transparency, Phys. Rev. Lett. **107**, 163604 (2011).

[30] N. Murata, R. Hata, and H. Ishihara, Crossover between energy transparency resonance and Rabi splitting in antenna-molecule coupled systems, J. Phys. Chem. C **119**, 25493 (2015).

[31] S. D. Sarma and W. Lai, Screening and elementary excitations in narrow-channel semiconductor microstructures, Phys. Rev. B **32**, 1401 (1985).

[32] A. R. Goni, A. Pinczuk, J. S. Weiner, J. M. Calleja, B. S. Dennis, L. N. Pfeiffer, and K. W. West, One-Dimensional Plasmon Dispersion and Dispersionless Intersubband Excitations in GaAs Quantum Wires, Phys. Rev. Lett. **67**, 3298 (1991).

[33] J. Hao and G. W. Hanson, Electromagnetic scattering from finite-length metallic carbon nanotubes in the lower IR bands, Phys. Rev. B **74**, 035119 (2006).

[34] J. Takahara, S. Yamagishi, H. Taki, A. Morimoto, and T. Kobayashi, Guiding of a one-dimensional optical beam with nanometer diameter, Opt. Lett. **22**, 475 (1997).

[35] F . K . Chang, F. J. García de Abajo, and F. J. G. De Abajo, Graphene plasmonics: A platform for strong light-matter interactions, Nano Lett. **11**, 3370 (2011).

[36] H. Yan, T. Low, F. Guinea, F. Xia, and P. Avouris, Tunable phonon-induced transparency in bilayer graphene nano- r (2014).

[37] L. Ju, B. Geng, J. Horng, C. Girit, M. Martin, Z. Hao, H. a Bechtel, X. Liang, A. Zettl, Y. R. Shen, and F. Wang, Graphene plasmonics for tunable terahertz metamaterials, Nat. Nanotechnol. **6**, 630 (2011).

[38] F. Koppens, M. B. Lundeberg, M. Polini, T. Low, and P. Avouris, in *2D Materials: Properties and Devices* (Cambridge University Press, Cambridge, England, 2017).

[39] K. J. Erikson, X. He, A. A. Talin, B. Mills, R. H. Hauge, T. Iguchi, N. Fujimura, Y. Kawano, J. Kono, and F. Léonard, Figure of merit for carbon nanotube photothermoelectric detectors, ACS Nano **9**, 11618 (2015).

[40] A. E. Nikolaenko, F. De Angelis, S. A. Boden, N. Papasimakis, P. Ashburn, E. Di Fabrizio, a I. Zheludev, Carbon Nanotubes in a Photonic Metamaterial, Phys. Rev. Lett. **104**, 153902 (2010).

[41] S. De Vega, J. D. Cox, and F. J. G. De Abajo, Plasmons in doped finite carbon nanotubes, and their interactions with fast electrons, and quantum emitters, Phys. Rev. B **94**, 075447 (2016).